Journal of Oceanology and Limnology

https://doi.org/10.1007/s00343-025-5260-4

Research Paper

Hydrology and sediment supply in the largest lake system of Qaidam Basin, northeastern Qinghai-Xizang Plateau: insights from surface-sediment grain size*

Hongyu LI[1, 2, 3], Haicheng WEI[1, 2, **], Aiying CHENG[1, 2], Chunliang GAO[1, 2], Chenyu WANG[1, 2, 3], Ronglei DUAN[1, 2, 3], Shun WANG[1, 2], Hongpan XUE[1, 2]

[1] *Key Laboratory of Green and High-end Utilization of Salt Lake Resources, Qinghai Institute of Salt Lakes, Chinese Academy of Sciences, Xining 810008, China*

[2] *Qinghai Provincial Key Laboratory of Geology and Environment of Salt Lakes, Chinese Academy of Sciences, Xining 810008, China*

[3] *University of the Chinese Academy of Sciences, Beijing 100049, China*

Received Jul. 10, 2025; accepted in principle Oct. 15, 2025; accepted for publication Nov. 22, 2025

Abstract Climate warming and increased precipitation across the Qinghai-Xizang Plateau (QXP) have caused lake expansion, posing a threat to the safety of local infrastructure and ecosystems. Grain size in lake sediments is a reliable proxy for elucidating hydrological variations in these lakes. However, diverse sources of clastic fractions in lake sediments complicate the interpretation of hydrological changes based on grain-size records. We analyzed 94 surface-sediment samples from Hurleg and Toson lakes, the largest lake system of the Qaidam Basin, northeastern QXP, and explored the grain-size spatial distribution and its hydrological significance. Results demonstrate that fine silt (4–16 μm) is predominant in both lakes, followed by medium to coarse silt (16–63 μm), and clay (<4 μm), while sand (>63 μm) fraction was the least abundant. Using the end-member analysis (EMA), we identified three end-members in Hurleg Lake (HEM1–HEM3) and four in Toson Lake (TEM1–TEM4). In Hurleg Lake, HEM1 and HEM2 mainly come from fluvial deposits from the Bayin River. HEM3 mainly comes from surface runoff and shoreline erosion. In Toson Lake, TEM1 represents typical lacustrine sediments, and TEM2 represents fine-grained terrestrial residual and gully input components. TEM3 originates mainly from aeolian transport and terrestrial residual. TEM4 is a dominant component of the subaqueous alluvial fan. Single-specimen unmixing suggested a differentiation between aeolian inputs and hydrodynamically sensitive components. Fine silt components (mode size 4.0–14.5 μm) are likely related to lake-level variations, whereas coarser silt components (mode size 18.7–51.8 μm) indicate regional dust activity. Notably, in Toson Lake, the fluvial sand components (mode size 66.9–111.5 μm) that were likely derived from western gully runoff, may represent a potential indicator of extreme hydrological events in the Qaidam Basin. These findings provide robust constraints on modern sedimentary processes for reconstructing the history of hydroclimatic changes using grain-size records in the northeastern QXP.

Keyword: Hurleg and Toson lakes; grain size; lake surface sediment; hydrology; Qaidam Basin

1 INTRODUCTION

The Qinghai-Xizang Plateau (QXP) is in average elevation over 4 000 m and characterized by its unique environment and climate, is often referred to as “the Third Pole” of the world (Qiu, 2008; Yao et al., 2012; Zhang et al., 2020; Yu et al., 2024). As the source of many major Asian rivers, the QXP provides fresh water for more than 2 billion people, earning the title of “Asian water tower” (Immerzeel et al.,

* Supported by the National Natural Science Foundation of China (No. 42172019), the Outstanding Youth Program of the Natural Science Foundation of Qinghai Province (No. 2023-ZJ-941J), and the Youth Interdisciplinarity Team of Fundamental Research, Qinghai Institute of Salt Lakes, Chinese Academy of Sciences (No. islJCTD-2022-1)

** Corresponding author: hcwei@isl.ac.cn

2010; Xu et al., 2019; Yao et al., 2022). It is not only the origin of these rivers but also home to the world's highest concentration of lakes (Feng et al., 1998; Wan et al., 2014; Xu et al., 2019). However, in recent decades, the lakes on the QXP have experienced significant expansion due to the warmer and wetter climate caused by anthropogenic emissions and forcing (Qin et al., 2005; Peng et al., 2018), posing threats to regional infrastructure and ecological security (Pekel et al., 2016; Xu et al., 2024). Lake expansion is projected to submerge critical human infrastructure, including roads, settlements, and ecological components such as grasslands, wetlands, and croplands (Xu et al., 2024). Understanding and reconstructing the hydrological characteristics of these lakes is crucial for predicting future changes in lacustrine hydrology.

Grain size in lake sediments provides rich information of sediment sources, lake-level changes, and hydrodynamic conditions (Middleton, 1976; Ashley, 1978; Vasskog et al., 2016; Liu et al., 2024). However, interpreting grain-size data can be challenging due to the complex and overlapping signals it contains. For instance, the silt fraction (4–63 μm) often preserves its original characteristics and has been linked to river inflow or runoff intensity in lakes such as Ebinur and Bosten in Arid Central Asia (Sun et al., 2002; Chen et al., 2006; Liu et al., 2016; Zhou et al., 2022). But the same fraction is also abundant in aeolian deposits like loess, where it can account for 17%–52% of lake sediments (Dong et al., 2017). Similarly, the sand fraction (>63 μm) is commonly used as an indicator to dust storm activity (Qiang et al., 2007; An et al., 2012; Chen et al., 2013; Wang et al., 2019; Zhang et al., 2022). However, in lakes with inflowing rivers, coarse sand is often delivered by extreme flood events (Walling and Moorehead, 1989; Sun et al., 2002; Dong et al., 2010; Dietze et al., 2014; Zhou et al., 2018; Wang et al., 2021). This overlap complicates efforts to separate hydrological signals from aeolian inputs. To address this issue, geochemical proxies offer valuable tools for identifying sediment sources and distinguishing between fluvial and aeolian contributions (Mulitza et al., 2008; Stuut et al., 2014; Du et al., 2018; Liu et al., 2020; Huyan and Yao, 2022; Li et al., 2023). Therefore, integrating grain-size analysis with geochemical data is essential for accurately reconstructing lake hydrodynamics and sediment provenance.

The Qaidam Basin, located in the northeastern QXP, is one of the world's driest regions (An et al., 2012; Yu and Lai, 2012). Following the disappearance of the mega-Qaidam Lake, the basin retained substantial lacustrine sediment (Chen and Bowler, 1986; Madsen et al., 2014). However, these paleolake sediments are frequently reworked by the wind into aeolian formations like dune sands and loess, making them unsuitable for studying lake sediment transport processes (Dong et al., 2017). Hurleg and Toson lakes, situated at the northeastern edge of the Qaidam Basin, form the largest lake ecosystem in the basin and are primarily influenced by mid-latitude westerlies outside the reach of the Asian summer monsoon (Huang et al., 2023). The closed lake system provides an ideal setting to study the evolution of the hydrological system in the northeastern QXP. At present, significant research has been conducted in this region, exploring hydroclimate change, vegetation succession, and lake evolution using pollen records (Zhao et al., 2007, 2010b; Yu et al., 2021), paleo-shorelines (Fan et al., 2014; Li et al., 2022), carbon and oxygen isotopes (Li et al., 2016; Zhao et al., 2022), sediment grain size (Ding et al., 2020; Song et al., 2020), and element intensities (Ling et al., 2018). However, the Holocene hydroclimate patterns reconstructed using different proxies often contradict each other. Grain-size records and multi-proxy humidity reconstructions suggest relatively dry conditions since the mid to late Holocene in the Hurleg and Toson Lake Catchment (Zhao et al., 2010a; Song et al., 2020), consistent with pollen records from eastern Gahai Lake sediments (Zhou et al., 2024). Nevertheless, these findings conflict with paleo-shoreline records, which indicate three high lake-level periods during the mid to late Holocene (Fan et al., 2014). Additionally, discrepancies exist in grain-size-based humidity reconstructions regarding the presence of a moderately humid period in the late Holocene (Cao et al., 2008; Chen et al., 2010; Song et al., 2020). The uneven distribution and multiple sources of sediments may contribute to this complexity. Ding et al. (2020) observed significant grain-size variation among parallel sediment cores from Toson Lake, highlighting the diversity of sediment sources and their complex spatial distribution. Zhang et al. (2022) used the coarse fraction (>63 μm) as an indicator of dust storms in Hurleg Lake, but inconsistencies of this fraction in parallel cores hindered the accurate reconstruction of dust activity intensity. Therefore, understanding modern processes of lacustrine sediment grain size will aid in clarifying the significance of different grain-size

components and improve the reconstruction of paleo-hydrological events and hydroclimates on the northeastern QXP.

This study collected lake surface sediments in dense networks from across Hurleg and Toson lakes to investigate grain-size spatial distribution, sediment transport trends, and sediment sources. We focus on our analyses on three key issues: (1) to reveal the spatial distribution patterns of grain-size fractions and parameters; (2) to decompose the grain-size signal, identify the sources and their hydrological indicators for each sensitive component; and (3) to classify the sedimentary environments and explore their indicative significance for paleo-hydroclimate in northeastern QXP.

2 MATERIAL AND METHOD

2.1 Regional characteristic

Hurleg Lake (37°14′N–37°20′N, 96°51′E–96°57′E) and Toson Lake (37°04′N–37°13′N, 96°50′E–97°03′E) are located at the northeastern edge of the Qaidam Basin in the northeastern QXP, within the western Delingha Subbasin (Fig.1a). Both lakes are situated at an elevation of approximately 2 800 m above sea level. Hurleg Lake covers an area of about 55 km, with an average depth of about 4.3 m and a maximum depth of 8 m. Toson Lake spans approximately 145 km^2 with an average depth of 20.9 m and a maximum of 32.2 m (Supplementary Table S1). Hurleg Lake is primarily fed by the Bayin River and drains through the Dalian River into Toson Lake. Additionally, a preliminary investigation identified a gully on the west side of Toson Lake (Li et al., 2025), which serves as a significant water source and material supplier during periods of extreme precipitation (Fig.1b).

The climate conditions in Hurleg and Toson lakes are characterized by high aridity with annual precipitation averages of about 103 mm, and the annual temperature is approximately 3 °C on average, according to data from the high-resolution near-surface meteorological forcing dataset for the Third Pole region (TPMFD) from 1979 to 2023 (Shao et al., 2022; Jiang et al., 2023, 2025; Yang et al., 2023). Most precipitation occurs as rain during the summer (Zhao et al., 2010b). The modern vegetation in this region is dominated by desert plant communities, mainly composed of Amaranthaceae species (including *Salsola abrotanoides*, *Salsola arbuscula*, *Kalidium gracile*, *Kalidium foliatum*, *Ceratoides aritim*, *Haloxylon ammodendron*, *Sympegma regelii*, and *Salicornia europaea*), *Ephedra*, *Nitraria tangutorum*, and *Artemisia*. The wetlands around the lakes and downstream of the Bayin River support a large number of hygrophytes, including *Phragmites*, Cyperaceae, and Hippuridaceae. Additionally, the Gobi Farm and Huaitoutala Town have farmlands where spring wheat (*Triticum aestivum*) and rape (*Brassica campestris*) are primarily cultivated (Zhao et al., 2007; Hou, 2019).

2.2 Fieldwork and laboratory treatment

In 2015 and 2023, we collected 25 surface-sediment samples from Hurleg Lake (H1–H25) and 69 from Toson Lake (T1–T69) with Ekman grab sampler. GPS and a bathymeter recorded the longitude, latitude, and water depth at each sampling site (Supplementary Table S1). The samples were placed in polyethylene bags and preserved at low temperatures in the laboratory.

2.2.1 Grain-size measurement

Grain-size distribution (GSD) was analyzed with a Malvern Mastersizer 3000 particle analyzer, which can detect particles ranging from 0.01 to 3 500 μm. Although the Malvern Mastersizer 3000 is a precise tool for particle size analysis, measurement errors can occur due to improper sample dispersion, refractive index settings, or poor sample preparation, particularly with fine-grained sediments. Its laser diffraction method assumes ideal particle shapes, which may result in inaccuracies for irregular or angular particles, especially in the silt and clay-size ranges. These factors can lead to misclassification of GSDs, making proper sample pretreatment essential.

Prior to analysis, dried samples (0.3–0.5 g) were pretreated to remove organic matter, carbonates, and iron oxides. Organic matter was removed by adding 30% H_2O_2, while 10% HCl was used to eliminate carbonates and iron oxides. To disperse clay particle aggregates, 10% $(NaPO_3)_6$ was added, and the samples were treated with ultrasonic dispersion and shaking (Lu and An, 1998; Wünnemann et al., 2023). To ensure stable results, each sample was measured three times, with intervals of 30 s, and the average value of these measurements was used as the final GSD result.

2.2.2 Geochemical analysis

To aid in identifying sediment provenance, five surface samples (G1–G5) were collected from a gully on the western margin of Toson Lake in 2025, along with 15 representative lacustrine samples

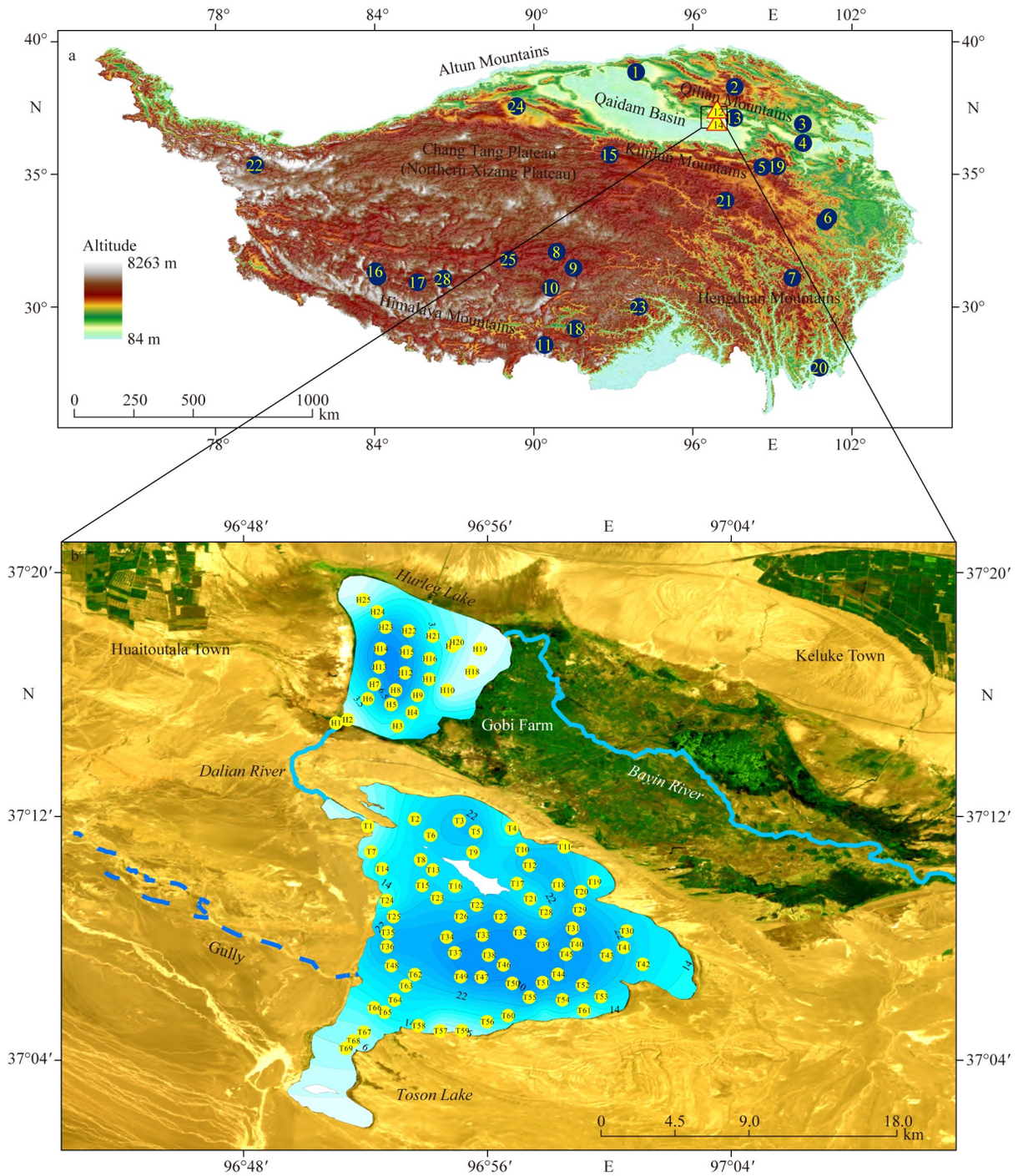

Fig.1 Study area and sampling locations

a. location of Hurleg and Toson lakes (triangles within the black box) in the Qaidam Basin, northeastern Qinghai-Xizang Plateau. Dark blue dots indicate sites of previously published lake sediment grain-size studies (see Supplementary Table S2 for references); b. bathymetric map of Hurleg and Toson lakes overlaid on a Landsat 9 satellite image (source: https://www.usgs.gov/). Yellow dots mark the surface sediment sampling sites (Supplementary Table S1).

from Hurleg and Toson lakes. All samples were air-dried, finely ground, and sieved through a 200-mesh screen (~75 μm) to ensure consistency. Geochemical compositions were then analyzed using a Vanta handheld X-ray fluorescence (XRF) analyzer. Zirconium (Zr), a chemically stable element, serves as an effective tracer for sediment source due to its resistance to weathering and its association with parent rock composition (Taylor and McLennan, 1985; McLennan, 1989). Silicon

dioxide (SiO_2) is sensitive to grain-size variations and provides insight into sedimentary processes (Pang et al., 2023). Therefore, both ZrO_2 and SiO_2 concentrations were measured to assist in differentiating lacustrine sediment sources.

2.3 Data analysis

2.3.1 Analysis and decomposition of GSD signal

To analyze the clastic fractions and grain-size parameters of surface sediments from Hurleg and Toson lakes, AnalySize-1.2.2 (a MATLAB R2019b-based tool) was utilized (Paterson and Heslop, 2015; The MathWorks Inc., 2019). The grain sizes were classified into four categories: clay (<4 μm), fine silt (4–16 μm), medium to coarse silt (16–63 μm), and sand (>63 μm), following the Udden-Wentworth standard (Udden, 1914; Wentworth, 1922; Ming et al., 2021). The mean grain size, sorting coefficient, skewness, and kurtosis were assessed using the statistical moment method of Krumbein and Pettijohn (1938). Additionally, we performed the end-member analysis (EMA) using the General Weibull (Gen. Weibull) distribution, which was selected for its location parameter that controls the limit of the left-hand tail of the distribution, affecting skewness (Weibull, 1951; Paterson and Heslop, 2015). The single-specimen unmixing of representative samples was also performed by fitting the Gen. Weibull distribution. This fitting was conducted using QGrain 0.2.4 software (Liu et al., 2021). This comprehensive approach allowed for accurate and detailed analysis of the sediment GSD and its implications for environmental changes.

2.3.2 Statistical method

The relative proportions of each grain-size component were evaluated using the log-ratio method following Yamaguchi et al. (2024). Because compositional data are constrained by a constant sum, the additive log-ratio (ALR) transformation was applied to express the relative relationships among components (Aitchison, 1986). One reference component is chosen as the denominator, and all other components are numerators. For J components with values X_1, X_2, ⋯, X_J, there are J–1 log ratios in the ALR set with respect to the selected reference component (ref) as follows:

$$\mathrm{ALR}(j|\mathrm{ref})=\ln(X_j/X_{\mathrm{ref}}) \text{ for } j=1, \cdots, J;\ j\neq\mathrm{ref}. \quad (1)$$

Prior to transformation, zero values were replaced by small positive numbers using the multiplicative replacement procedure (Martín-Fernández et al., 2003) to avoid undefined logarithmic terms. The most stable component was selected as the reference term (X_{ref}) based on the approach of Ohta et al. (2011), which identifies the least variable fraction through comparison of the coefficient of variation (CV) ratios among all components. This allowed the transformed data to represent the relative enrichment or depletion of each component with respect to the stable reference, minimizing the effects of closure and enabling quantitative comparison of compositional variability. This method serves as a supplementary approach to the EMA results, providing additional insight into the relative variability among grain-size components.

Ordination analysis was employed to examine the relationship between environmental factors and grain-size components. Detrended correspondence analysis (DCA) was performed using data for grain-size components and environmental variations. The DCA results indicated that the gradient lengths of the first four axes of variation in both lakes were less than two standard deviation units, suggesting linear underlying responses. Consequently, the relationships between grain-size components and environmental variations were evaluated using principal component analysis (PCA) in Origin 2021 (OriginLab Corporation, 2020). Water depth, distance to the estuary, and offshore distance were used as supplementary variables. For Hurleg Lake, the distance to the estuary represents the distance between the sampling site and the Bayin River estuary. For Toson Lake, the distance to the estuary denotes the distance between the sampling site and the Dalian River estuary, while the distance to the gully estuary was also considered an important variable.

GiSedTrend (GIS-based sediment trend analysis), based on QGIS 2.18 (QGIS Development Team, 2016), was used to explore sediment transport trends in Hurleg and Toson Lakes. This analysis focused on surface sediment grain-size parameters, including mean grain size, sorting coefficient, and skewness (Poizot and Méar, 2010). Additionally, we performed systematic cluster analysis using *hclust* function in R (R Core Team, 2023) to classify the sedimentary environments of Hurleg and Toson lakes. R-type clusters are used to sift effective variables, and Q-type clusters are used to classify samples based on multiple variables (Li et al., 2015). This comprehensive approach allowed for detailed understanding of the sedimentary processes and environmental influences in the study area.

3 RESULT

3.1 Spatial distribution of clastic fraction

The grain size of surface-sediment samples from Hurleg Lake ranged 0.5–586.0 μm, on average of 10.6 μm, while those from Toson Lake ranged 0.5–976.5 μm, on average of 11.5 μm. Overall, sediments in Toson Lake are slightly coarser than those in Hurleg Lake. Fine silt is the dominant fraction in both lakes, followed by medium to coarse silt and clay fractions. Ultimately, the sand content covers the lowest percentage (Table 1). Despite a slight variation in grain-size proportion, both lakes share a similar sediment composition.

In Hurleg Lake, the clay fraction is notably higher near the northeastern lake shore and the lake outlet, extending in a tongue shape toward the depocenter (Fig.2a). The distribution of the fine silt fraction resembles that of clay, with high-value areas near the northeastern and southern shorelines (Fig.2b). Medium to coarse silt is found predominantly in the northwestern and southeastern areas, contrasting with the clay and fine-silt fractions (Fig.2c). Sand, being the lowest content, is distributed in a circular pattern from the shore to the center, with notable concentrations at two points on the southeastern shore (Fig.2d).

In Toson Lake, the clay fraction is widespread, with the highest content in three depocenters (Fig.2a). Fine silt predominates along the northeastern shore and gradually decreases towards the southwest (Fig.2b). Medium to coarse silt accumulates along

Table 1 Grain-size composition of surface-sediment samples

Class	Hurleg Lake				Toson Lake			
	Min. (%)	Max. (%)	Average (%)	Standard division (%)	Min. (%)	Max. (%)	Average (%)	Standard division (%)
Clay	7.9	33.9	20.4	7.1	7.4	30.0	20.6	4.9
Fine silt	31.2	56.2	42.7	6.7	27.4	55.3	42.2	6.8
Medium to coarse silt	14.4	40.2	27.1	7.8	13.6	36.5	22.5	4.1
Sand	1.2	20.8	6.2	4.5	1.4	36.2	10.9	6.9

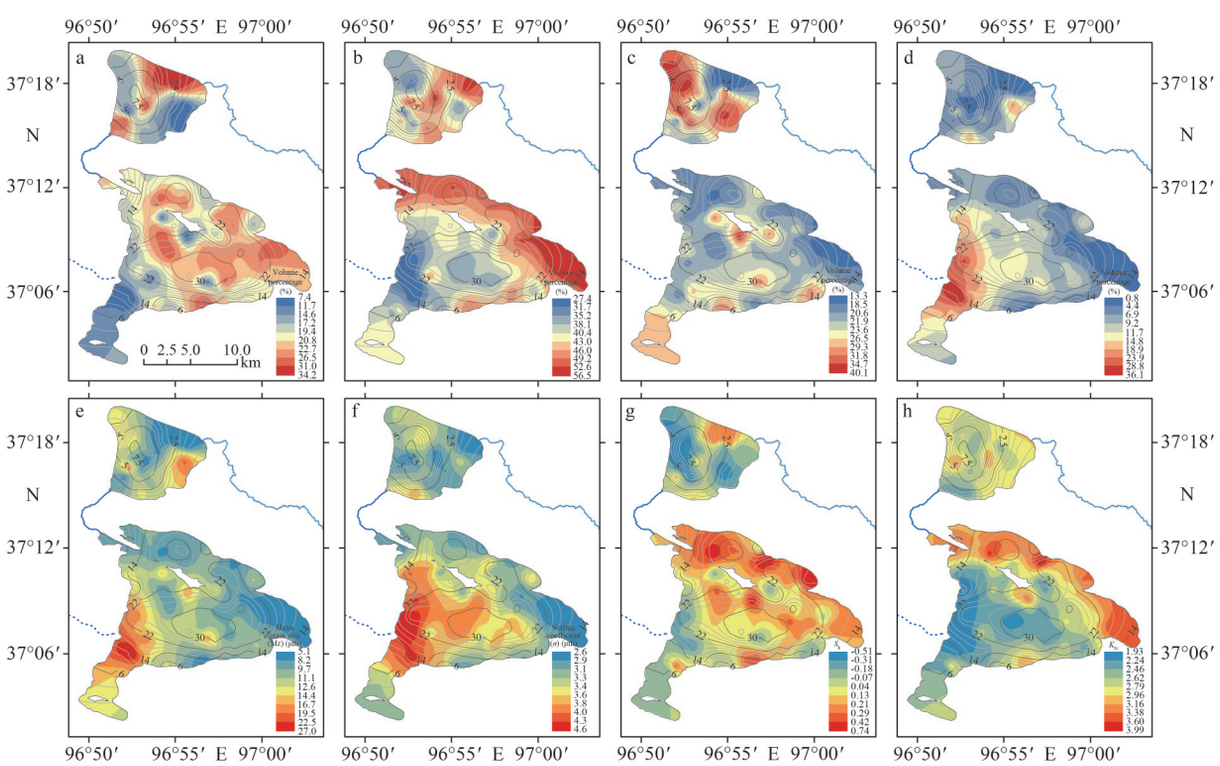

Fig.2 Spatial distribution of grain-size fractions and parameters in surface sediments from Hurleg and Toson lakes

a. clay; b. fine silt; c. medium to coarse silt; d. sand fractions; e. mean grain size (Mz); f. sorting coefficient (σ); g. skewness (S_k); h. kurtosis (K_G).

the southern shoreline and around the central island, with significant amounts in the southern depocenter (Fig.2c). The sand fraction is prominent in the western area of Toson Lake, extending fan-shaped from the gully outlet to the southern depocenter (Fig.2d).

3.2 Spatial distribution of grain-size parameters

Grain-size parameters, including mean grain size, sorting coefficient, skewness, and kurtosis, provide insights into the material sources, transport mechanisms, and depositional environments of sediments.

In Hurleg Lake, mean grain size varies from 6.0 to 20.5 μm, on average of 10.6 μm. Higher values are found in the northwestern and southeastern areas, while lower values are in the northeast and southwest regions (Fig.2e). In Toson Lake, mean grain size ranges from 6.1 to 27.1 μm, with an average of 11.5 μm. The western lakeshore near the gully estuary shows higher values (Fig.2e). The coarse fraction significantly influences mean grain size in both lakes.

The sorting coefficient reflects the degree of sediment sorting, with values between 0.5 and 1.0 μm indicating moderate sorting, values above 1.0 μm indicating poor sorting, and values below 0.5 μm indicating well-sorted sediments (Folk and Ward, 1957; McManus, 1988). In Hurleg Lake, the sorting coefficient ranges 2.6–3.8 μm, average of 3.2 μm, indicating surface sediments in this lake are poorly sorted. The poorest sorting is observed in the northern basin and along the southern shoreline (Fig.2f). Toson Lake also exhibits poorly sorted sediments, with coefficients ranging from 2.6 to 4.6 μm on average of 3.5 μm. The most poorly sorted sediments are found near the western shoreline, extending from the gully estuary to the depocenter (Fig.2f).

Skewness reflects the asymmetry of GSD. In Hurleg Lake, skewness values range from -0.5 to 0.3, on average of -0.1. Positive skewness, indicating a dominance of finer particles, is observed near the northern and southern shorelines (Fig.2g). In contrast, negative skewness occurs in the northwestern region, suggesting a shift toward coarser grains likely caused by a sudden decrease in flow velocity. In Toson Lake, skewness ranges from -0.2 to 0.7, averaging 0.1. Positive skewness dominates the central area, where finer sediments are concentrated (Fig.2g). Negative skewness near the gully outlet corresponds with higher sand content, pointing to localized coarse sediment input.

Kurtosis describes the sharpness or peakedness of the GSD. In Hurleg Lake, kurtosis ranges from 2.3 to 3.4, with an average of 2.7. Most sediments exhibit a leptokurtic or very leptokurtic distribution, particularly within the 2.8–3.2 range (Fig.2h). In Toson Lake, kurtosis values range from 1.9 to 4.0, averaging 2.7. Higher kurtosis (>2.8) along the northeastern shore suggests less modification of surface sediments. Conversely, lower kurtosis (<0.9) in the southern depocenter and western area reflects a mesokurtic distribution, likely resulting from complex transport processes involving strong fluvial or aeolian activity (Fig.2h).

3.3 Decomposition of the grain-size components

The Gen. Weibull function provides a stable and reliable fit for unmixing multiple end-members, especially when dealing with three or more end-members, which yields less scattered abundance results compared to other methods and is effective in capturing the main trends of the data (Paterson and Heslop, 2015). To determine the number of end-members before performing the EMA using the Gen. Weibull function, we analyzed the linear correlation and angular deviation of the dataset. Selecting a minimized number of end-members with a high linear correlation and low angular deviation ensures a better fit between the measured grain-size curve and the end-members. R^2 of each cluster exceeds 0.95 at the 95% confidence level, indicating an excellent fit with an angular deviation of less than 5 (Supplementary Fig.S1). In Hurleg Lake sediments, we identified three end-members (HEM1–HEM3) (Fig.3a), while in Toson Lake sediments, we identified four end-members (TEM1–TEM4) (Fig.3b). The mode size of an end-member reflects the dominant transport and deposition processes.

In Hurleg Lake, HEM1 represents fine-grained offshore suspension deposits with a mode size of 2.1 μm (clay). It exhibited high concentrations near the northeastern lakeshore and the lake outlet, forming distinct tongue- and fan-shaped distribution patterns, respectively (Fig.4a). HEM2, characterized by a mode size of 6.7 μm (fine silt), also represents offshore suspension and was concentrated near the Bayin River estuary and the southern shoreline, extending toward the depocenter (Fig.4b). HEM3, the predominant component in Hurleg Lake sediments, has a mode size of 24.1 μm (medium silt). It exhibited high proportions in the northwestern and southeastern areas of the lake, extending from the

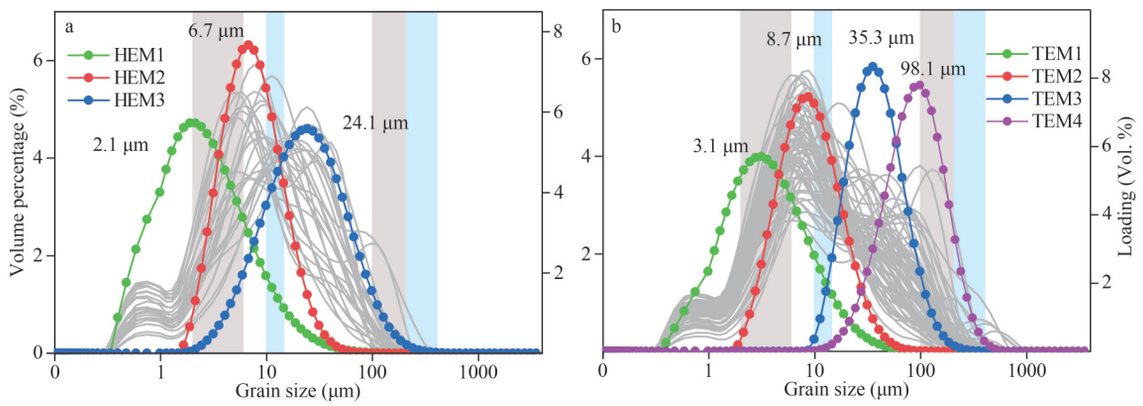

Fig.3 End-member loadings derived from surface sediments of Hurleg (a) and Toson (b) lakes

Blue shaded areas indicate typical grain-size ranges of fluvial deposits, including suspension (10–15 μm) and saltation (200–400 μm) components (Sun et al., 2002; Opluštil et al., 2005). Gray shaded areas represent typical aeolian grain-size ranges, including fine (2–6 μm) and coarse sand (100–200 μm) components (Walker and James, 1992; Sun et al., 2002).

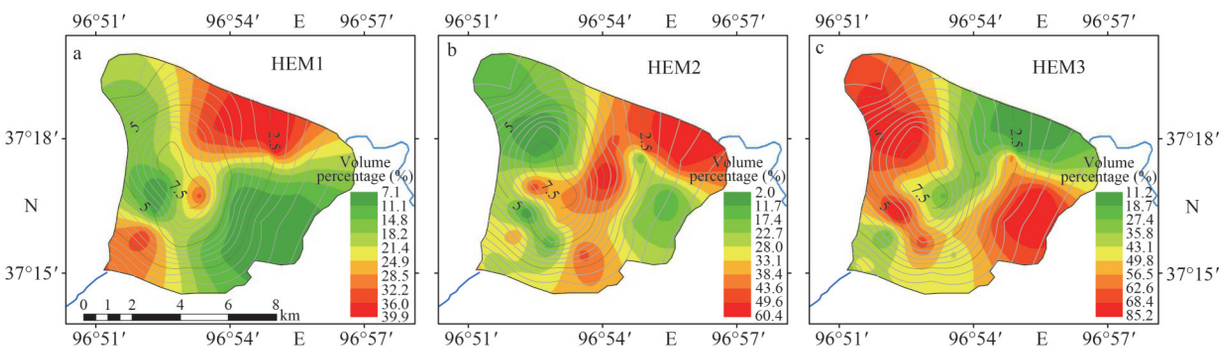

Fig.4 Spatial distribution of the three end-members identified in surface sediments from Hurleg Lake

a. HEM1; b. HEM2; c. HEM3.

shoreline toward the depocenter (Fig.4c).

In Toson Lake, TEM1 represents fine-grained offshore suspension deposits, with a mode size of 3.1 μm (clay), and is concentrated in three depocenters (Fig.5a). TEM2, with a mode size of 8.7 μm (fine silt), is the dominant component in Toson Lake sediments and primarily represents nearshore suspension deposits which concentrated along the northeastern shoreline (Fig.5b). TEM3, characterized by a mode size of 35.3 μm (medium silt), was primarily distributed along the southern shoreline, around the central island, and in parts of the southern depocenter (Fig.5c). TEM4, with a mode size of 98.1 μm (sand), represents nearshore saltation deposits. It forms a subaqueous fan extending from the gully outlets towards the southern depocenter (Fig.5d).

4 DISCUSSION

4.1 Origin of the grain-size end-members

The origins of individual end-members were identified using ALR analysis. In Hurleg Lake, the most stable of the three end-members, HEM1, was determined following the approach of Ohta et al. (2011). The fine-grained and even distribution component likely reflects fluvial deposits reworked by the lake currents and waves, long-range aeolian input, or materials formed through chemical weathering within the lake (Sun et al., 2002; Kasper et al., 2012; Dietze et al., 2014; Opitz et al., 2016; Liu et al., 2024; Yamaguchi et al., 2024). PCA results show a negative correlation between HEM1 proportion and distance to the estuary (Fig.6a), indicating that HEM1 mainly originates from Bayin River inflow and represents the typical fine-grained lacustrine sediments of Hurleg Lake.

Using HEM1 proportion as the X_{ref}, ALR (HEM2) revealed high-value areas near the Bayin River estuary and southeastern lake region, extending from the shoreline toward the depocenter in a tongue-shaped pattern (Fig.7a). The negative correlation between HEM2 and distance to the estuary (Fig.6a) suggests that HEM2 primarily consists of fine-silt

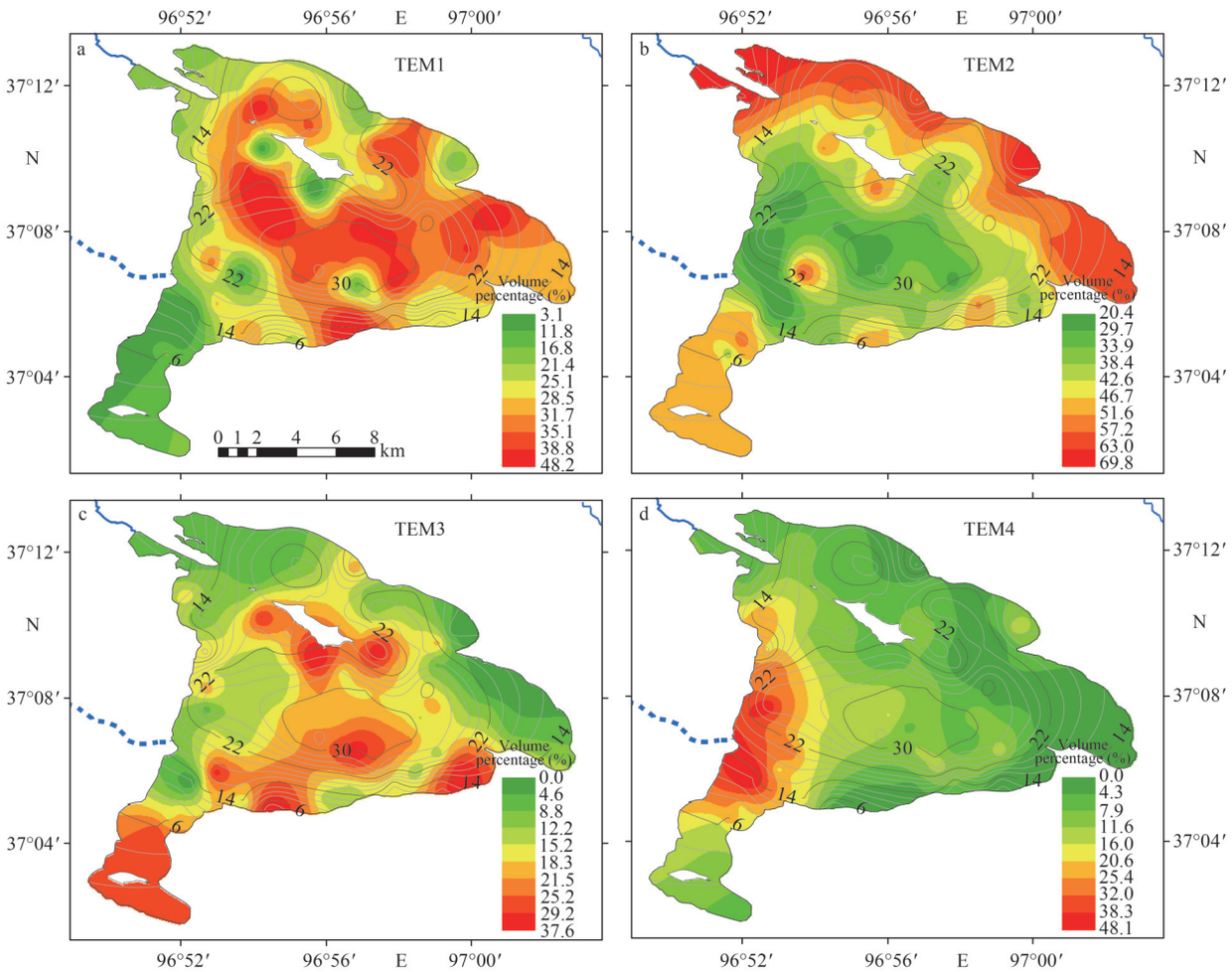

Fig.5 Spatial distribution of the four end-members identified in surface sediments from Toson Lake

a. TEM1; b. TEM2; c. TEM3; d. TEM4.

fractions from Bayin River deposits, forming a key component of the subaqueous alluvial fan in Hurleg Lake.

The spatial distributions of ALR (HEM3) and HEM3 patterns are basically consistent, with high values in the northwestern and southeastern regions extending toward the depocenter (Fig.7b). The coarse and fine tails of HEM3 (Fig.3a) indicate transport by multiple processes. Surface runoff and shoreline erosion are major contributors, while aeolian input also plays a role, as its mode size falls within the typical loess range (Pye, 1987; Tsoar and Pye, 1987; Sun et al., 2002; Dietze et al., 2014; Stauch et al., 2018).

Generally, sediments in Hurleg Lake are strongly influenced by the Bayin River. The spatial distribution of the three end-members reflects a current pattern dominated by river inflow. As fluvial deposits enter the lake, they move from the estuary along the eastern shore, depositing the coarse fraction and forming a subaqueous alluvial fan along the southeastern shore (Fig.1b). The finer fractions continue to migrate northward, settling along the northern coast. Ultimately, wind-induced sediment resuspension migrates these components to the depocenter (Supplementary Fig.S2).

In Toson Lake, TEM1 corresponds to HEM1, as both exhibit similar mode size and even distributions (Fig.3). Therefore, TEM1 mainly represents typical fine-grained sediments composed of fine suspended materials delivered by fluvial and surface runoff, and serving as the X_{ref} in ALR analysis. The distribution pattern of ALR(TEM2) has large differences from that of the TEM2 proportion, with high-value areas near the gully estuary, the southwestern bay, around the central island, and along the northeastern shoreline (Fig.7c). This pattern indicates that TEM2 consists of fine-grained materials from gully inflow, residual terrestrial deposits, and collapse of the Neogene lacustrine

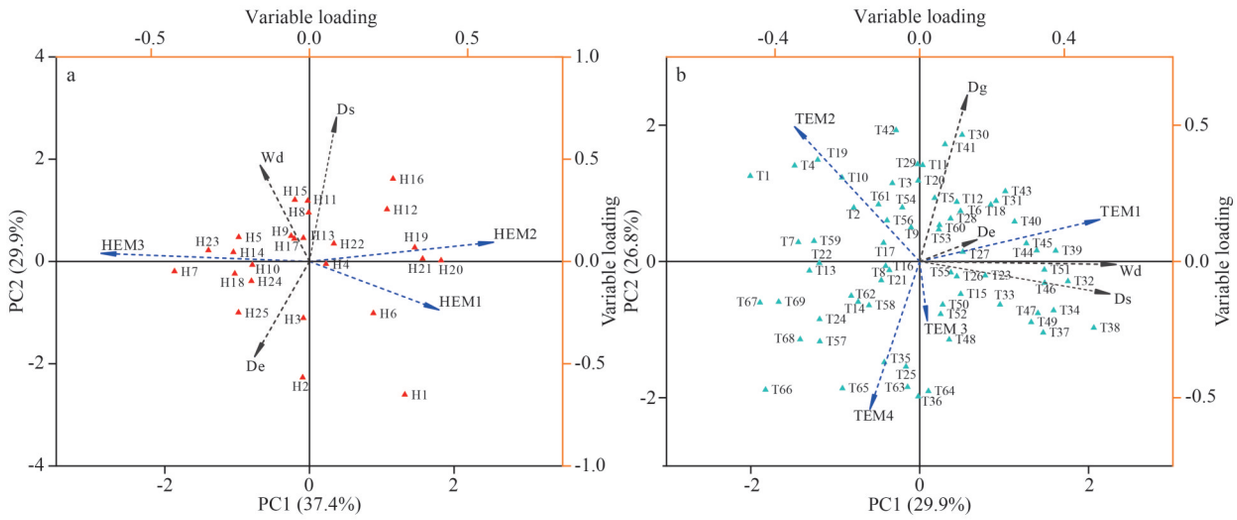

Fig.6 Principal component analysis (PCA) of grain-size end-members in Hurleg (a) and Toson (b) lakes

Supplementary variables include water depth (Wd), distance to the estuary (De), and offshore distance (Ds). For Toson Lake, the distance to the gully estuary (Dg) is also included as a key variable. The bottom and left axes represent the sample scores, while the top and right axes represent the variable loadings.

terrace. The rapid lake-level rise between 2018 and 2021 likely preserved these terrestrial materials in the southwestern lake bay and around the central island (Ma et al., 2022), expanding high-energy zones toward the present shoreline.

ALR (TEM3) exhibits a spatial distribution similar to ALR (TEM2), with high values in the southwestern bay and around the central island (Fig.7d), indicating TEM3 is also mainly composed of terrestrial residues. However, TEM3 shows lower values near the gully outlet and higher values across the lake, particularly in the southern depocenter (Fig.7d). This pattern suggests that TEM3 in the lake basin primarily originated from aeolian transport. The mode size of TEM3 also confirms this interpretation, which corresponds to typical loess deposits (Pye, 1987; Tsoar and Pye, 1987; Sun et al., 2002; Dietze et al., 2014; Stauch et al., 2018). ALR (TEM4) demonstrates a similar spatial distribution to the TEM4 proportion, concentration along the western shoreline, and extending from the gully outlet to the southern depocenter (Fig.7e). PCA results reveal a negative correlation between TEM4 and distance from the gully outlet (Fig.6b), confirming that this end-member is primarily supplied by gully transport.

4.2 Sedimentary zone division

The R-type cluster analysis indicated that the proportions of each grain-size fraction serve as valid proxies for classifying the sedimentary zones (Supplementary Fig.S3). Therefore, we used the grain-size fractions to perform the Q-type cluster, and both lakes could be divided into three zones respectively. Hurleg Lake sedimentary zones (HSZ) were identified as HSZ1, HSZ2, and HSZ3. Toson Lake sedimentary zones (TSZ) were identified as TSZ1, TSZ2, and TSZ3 (Fig.8a).

In Hurleg Lake, HSZ1 is located near the northeastern lakeshore and the Bayin River estuary, extending from the northeast to the depocenter (Fig.8a). This area primarily comprises clay and fine silt, and its distribution pattern overlaps with high-value areas of HEM1 (Fig.4a), indicating that fine-grained fluvial deposits dominate this area. HSZ2 is found in the northwestern and southeastern areas (Fig.8a), where sediments are dominated by medium to coarse silt. Considering this area overlaps with high value areas of ALR (HEM2) and ALR (HEM3) (Fig.7a & b), it primarily deposits clastic material brought into the lake by a relatively coarse fraction of the Bayin River, shoreline erosion, and aeolian deposits. HSZ3, with an average sand proportion of 16.9%, is situated along the southeastern lakeshore (Fig.8a). The sediment transport trend analysis revealed that in the shallow water areas of HSZ2, sediments exhibit a significant transport trend from the coast to the depocenter (Fig.8b), indicating wind-induced waves and currents had a significant impact on clastic distribution and resuspension (Jalil et al., 2019; Tang et al., 2020).

In Toson Lake, TSZ1 dominates the depocenters of the lake and covers the largest area (Fig.8a). It primarily comprises clay and fine silt and represents

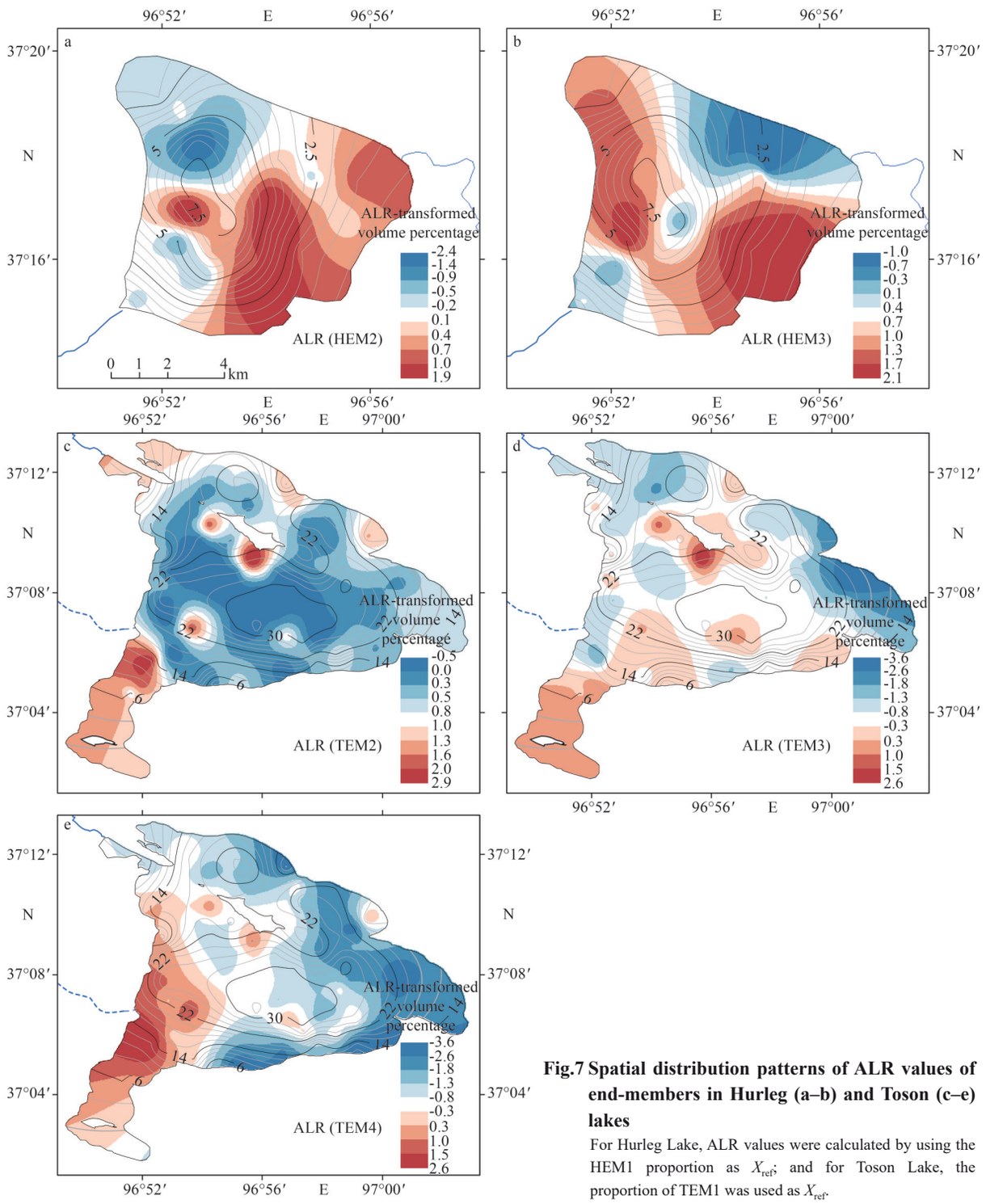

Fig.7 Spatial distribution patterns of ALR values of end-members in Hurleg (a–b) and Toson (c–e) lakes

For Hurleg Lake, ALR values were calculated by using the HEM1 proportion as X_{ref}; and for Toson Lake, the proportion of TEM1 was used as X_{ref}.

a typical lacustrine sedimentary environment. TSZ3, situated along the southwestern lakeshore near the gully outlet (Fig.8a), is a subaqueous alluvial fan, where the sediment transport trend is most pronounced, indicating a strong hydrodynamic intensity in this area (Fig.8b). TSZ2, located in the southwestern lake bay, around the big central island, and the dominant part formed the transitional zone between TSZ1 and TSZ3 (Fig.8a). In TSZ2, typical lacustrine sediments mixed with coarse-grained components from the gully input. This gradient confirms general hydrodynamic sorting during

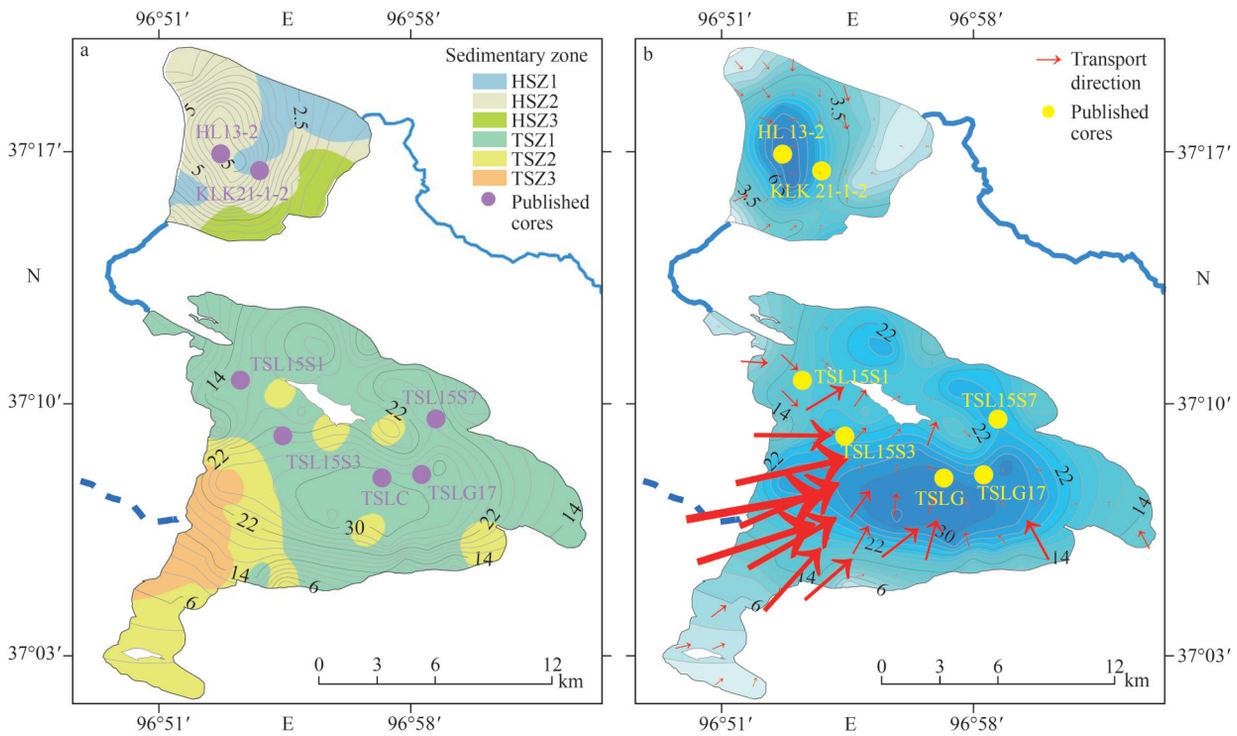

Fig.8 Representative sedimentary zones in Hurleg and Toson lakes (a) and the clastic transport trends of surface sediments in both lakes (b)

The arrow size represents the significance of the transport trend but the magnitude of the transport rate, and the arrow indicates the direction of sediment transport. The reference scale of Hurleg Lake is $1:1\times10^6$, and for Toson Lake is $1:5\times10^5$. Purple and yellow dots represent the locations of previously published core sediment sampling sites: HL 13-2 and KLK 21-1-2 (Zhang et al., 2022); TSLC (Fu et al., 2016); TSL15S1, TSL15S3, TSL15S7, and TSLG17 (Ding et al., 2020).

sediment transport within the lake (Xiao et al., 2012, 2015).

4.3 Distinguishing aeolian and hydrodynamically sensitive components in surface sediments

Quantifying the contributions of aeolian and hydrodynamic processes to sediment grain-size distributions is essential for interpreting paleo-hydroclimatic signals from core sediments. Based on the sedimentary zoning definition, we selected 15 representative sites in Hurleg Lake and 26 in Toson Lake, covering both subaqueous alluvial fans and depocenters (water depths>3.5 m in Hurleg Lake and >22 m in Toson Lake). Single-specimen unmixing results enabled us to characterize the mode size and volumetric contribution of both windborne and fluvial sediment inputs.

4.3.1 Identification of aeolian components

Single-specimen unmixing distinguished four distinct components from the Hurleg Lake depocenter (Fig.9a & b). C1 consists of ultra-fine clay-sized particles (mode size of 0.8–0.9 μm), likely derived from atmospheric deposition, fine-grained fluvial input, and authigenic processes (Sun et al., 2002; Xiao et al., 2007; Wang et al., 2021; Zhang et al., 2022). C2 is composed of fine silt (mode size of 4.0–14.5 μm), probably transported by rivers, dust fallout, and surface runoff (Dietze et al., 2014), then sorted and concentrated in the depocenter by hydrodynamic processes. This component typifies lacustrine deposition and serves as a sensitive proxy for lake-level fluctuations. C3 comprises medium to coarse silt (mode size of 18.7–51.8 μm) with its mode size in the range of typical loess, suggesting a possible aeolian contribution. C4 consists of sand-sized particles (mode size of 111.5–309.5 μm), which could be introduced by both episodic runoff and intense dust events. An appreciable amount of C4 in the depocenter suggests episodic deposition linked to extreme dust storms (Fig.9b). A similar grain-size pattern was observed in Toson Lake, where four primary components were also identified (Fig.9a & e). Here, C1 (mode size of 0.8–1.0 μm) and C2 (mode size of 4.6–5.9 μm) represent ultra-fine particles and typical lacustrine sediments,

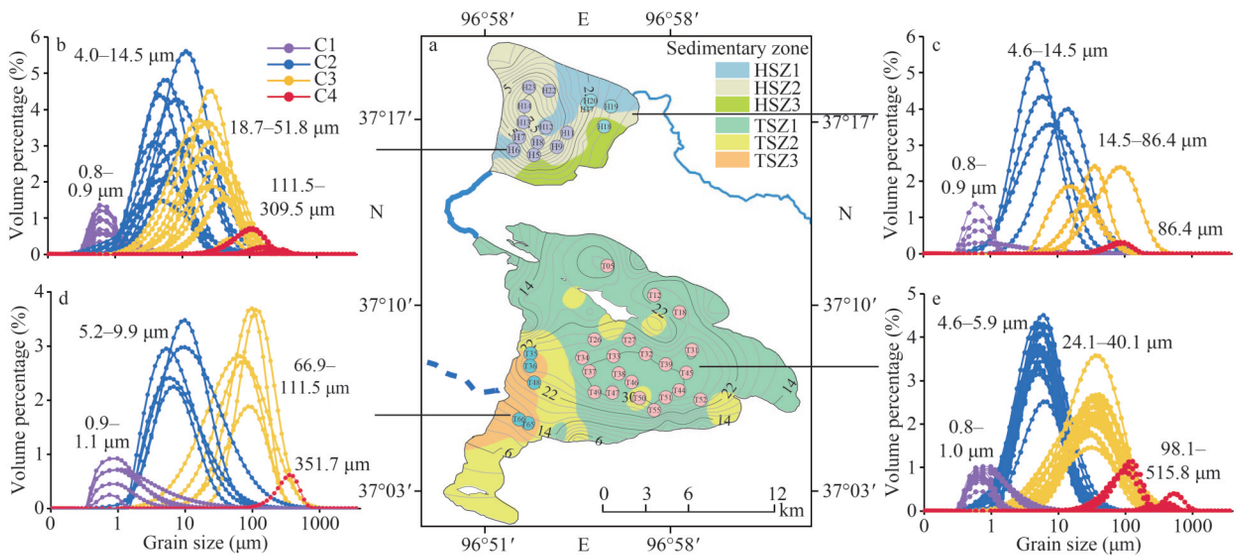

Fig.9 Summary of single-specimen unmixing results for surface sediments in Hurleg and Toson lakes

a. locations of representative surface-sediment samples; b. decomposition results from depocenter samples in Hurleg Lake; c. decomposition results from surface sediments near the Bayin River estuary in Hurleg Lake; d. decomposition results from the subaqueous alluvial fan in Toson Lake; e. decomposition results from depocenter samples in Toson Lake.

respectively. C3 (mode size of 24.1–40.1 μm) consists of TEM3, appears to reflect regional aeolian deposition, while C4 (mode size of 98.1–515.5 μm) likely represents material deposited during extreme dust storms.

4.3.2 Identification of hydrodynamically sensitive components

Surface-sediment samples from the subaqueous alluvial fan in Hurleg Lake are mainly composed of four grain-size components, similar in composition to those in the depocenter (Fig.9b & c). However, the C3 component in this area exhibits a wider range of variation (mode size of 14.5–86.4 μm) (Fig.9c), implying a mixture of fluvial and aeolian inputs. The partial overlap between C2 (mode size of 4.6–14.5 μm) and C3 suggests that lake hydrodynamics may have partially overprinted the original sedimentary signals (Fig.9c). Minimal spatial variation in ZrO_2 and SiO_2 concentrations across different sedimentary zones demonstrates that strong hydrodynamic processes have modified the original signals of grain-size in surface sediments (Fig.10b).

In Toson Lake, grain-size characteristics reflect a significant influence of hydrodynamic sorting. In the western subaqueous alluvial fan (TSZ3), the C2 component has a mode size of 5.2–9.9 μm (Fig.9d), approximately 1.5 times coarser than in the southern depocenter (mode size of 4.6–5.9 μm) (Fig.9e). Notably, the C3 component in TSZ3 has a mode size of 66.9–111.5 μm and accounts for an average of 44.4% of the sediment, clearly distinguishing it from the finer, aeolian-derived C3 in the southern depocenter (Fig.9d & e). Geochemical tracers reinforce this interpretation. ZrO_2 and SiO_2 decrease from the western gully toward the southern depocenter (Fig.10c), suggesting that C3 in TSZ3 is mainly influenced by fluvial input. Based on these findings, the C3 fraction with a mode size of 66.9–111.5 μm in TSZ3 may represent episodic coarse material deposited during flood events, potentially serving as a proxy for extreme hydrological events within the catchment. Moreover, the grain-size components in Toson Lake are more distinctly separated than those in Hurleg Lake (Fig.9b & e), indicating that Toson Lake sediments are better suited to preserve hydroclimatic signals in the Qaidam Basin.

5 CONCLUSION

This study analyzed the grain-size spatial distribution of surface sediments in Hurleg and Toson Lakes, interpreting sediment sources by decomposing grain-size components. These components provide valuable insights into paleo-hydroclimate reconstruction, improving our understanding of how lakes in the northeastern QXP respond to large-scale hydroclimate change.

In Hurleg Lake, HEM1 represents typical lacustrine sediments mainly transported by the Bayin River, and HEM2 is a coarser component that reflects Bayin River input, while HEM3 reflects a combination of surface runoff, shoreline erosion,

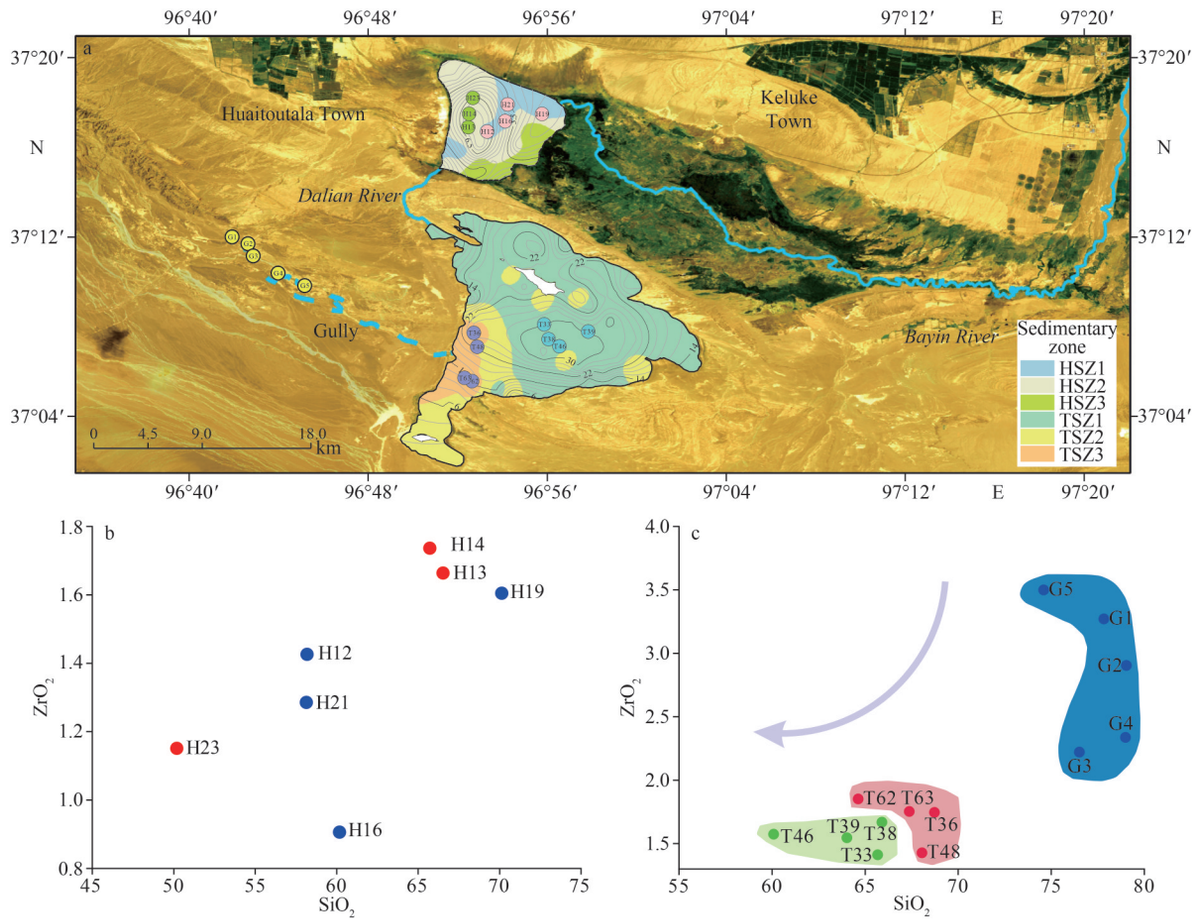

Fig.10 Locations of surface sediment samples selected by sedimentary zone for XRF analysis (a), concentrations of ZrO_2 and SiO_2 in surface sediments of Hurleg Lake (b), and those in Toson Lake (c), showing distinct spatial sorting patterns

All concentration values ($\times 10^{-6}$) are Hellinger-transformed.

and aeolian input. In Toson Lake, TEM1 corresponds with HEM1, representing typical lacustrine sediments, and TEM2 represents fine-grained gully input and terrestrial residue, as well as some of the Neogene lacustrine residue. TEM3 originates mainly from aeolian transport and terrestrial residue, and TEM4, a key constituent of the subaqueous alluvial fan, is predominantly derived from gully inflow.

Grain-size characteristics further allowed us to identify major sedimentary zones within each lake. In Hurleg Lake, the HSZ1 zone is dominated by fine sediments from fluvial input, while HSZ2 is enriched in medium to coarse silt of both aeolian and fluvial origin. In Toson Lake, TSZ1 represents the central lacustrine depositional area, TSZ3 the subaqueous alluvial fan, and TSZ2 the transitional zone between the two zones.

Single-specimen unmixing revealed that fine silt components (mode size of 4.0–14.5 μm) serve as a reliable proxy for lake-level changes, while medium to coarse silt (mode size of 18.7–51.8 μm) is likely related to regional dust activity. Notably, grain-size components with a mode size ranging between 66.9 and 111.5 μm in the western area of Toson Lake are transported via gully runoff and provide a sensitive proxy of flood events in the Qaidam Basin.

6 DATA AVAILABILITY STATEMENT

The datasets generated during and/or analyzed during the current study are available from the corresponding author on reasonable request.

References

Aitchison J. 1986. The Statistical Analysis of Compositional Data. Chapman and Hall, London. 400p.

An F Y, Ma H Z, Wei H C et al. 2012. Distinguishing aeolian signature from lacustrine sediments of the Qaidam Basin in northeastern Qinghai-Tibetan Plateau and its

palaeoclimatic implications. *Aeolian Research*, **4**: 17-30, https://doi.org/10.1016/j.aeolia.2011.12.004.

Ashley G M. 1978. Interpretation of polymodal sediments. *The Journal of Geology*, **86**(4): 411-421, https://doi.org/10.1086/649710.

Cao G C, Ma H Z, Long H et al. 2008. Particle size characteristics of deposits from DG03 core of Gahai Lake in east of Qaidam Basin and their environmental significance. *Journal of Desert Research*, **28**(6): 1073-1077. (in Chinese with English abstract)

Chen B S, Pan A D, Zhang Y F. 2010. Grain-size characteristics and their environmental significance of Gahai Lake sediments in Qaidam Basin. *Marine Geology & Quaternary Geology*, **30**(2): 111-119, https://doi.org/10.3724/SP.J.1140.2010.02111. (in Chinese with English abstract)

Chen F H, Huang X Z, Zhang J W et al. 2006. Humid Little Ice Age in arid Central Asia documented by Bosten Lake, Xinjiang, China. *Science in China Series D*: *Earth Sciences*, **49**(12): 1280-1290, https://doi.org/10.1007/s11430-006-2027-4.

Chen F H, Qiang M R, Zhou A F et al. 2013. A 2000-year dust storm record from Lake Sugan in the dust source area of arid China. *Journal of Geophysical Research*: *Atmospheres*, **118**(5): 2149-2160, https://doi.org/10.1002/jgrd.50140.

Chen K Z, Bowler J M. 1986. Late Pleistocene evolution of salt lakes in the Qaidam Basin, Qinghai Province, China. *Palaeogeography*, *Palaeoclimatology*, *Palaeoecology*, **54**(1-4): 87-104, https://doi.org/10.1016/0031-0182(86)90119-7.

Dietze E, Maussion F, Ahlborn M et al. 2014. Sediment transport processes across the Tibetan Plateau inferred from robust grain-size end members in lake sediments. *Climate of the Past*, **10**(1): 91-106, https://doi.org/10.5194/cp-10-91-2014.

Ding Z Y, Zhang J W, Yang P P et al. 2020. Comparison of sediment proxies of cores and their environmental significance at different locations of Lake Toson in Qaidam Basin. *Journal of Lake Sciences*, **32**(1): 259-270, https://doi.org/10.18307/2020.0124. (in Chinese with English abstract)

Dong J B, An Z S, Lu F Y. 2010. Quantitively partition of eolian and hydromorphic components in lacustrine sediments: an example from Lake Qinghai. *Journal of Geomechanics*, **16**(4): 402-411, https://doi.org/10.3969/j.issn.1006-6616.2010.04.008. (in Chinese with English abstract)

Dong Z B, Hu G Y, Qian G Q et al. 2017. High-altitude aeolian research on the Tibetan Plateau. *Reviews of Geophysics*, **55**(4): 864-901, https://doi.org/10.1002/2017RG000585.

Du S S, Wu Y Q, Tan L H. 2018. Geochemical evidence for the provenance of aeolian deposits in the Qaidam Basin, Tibetan Plateau. *Aeolian Research*, **32**: 60-70, https://doi.org/10.1016/j.aeolia.2018.01.005.

Fan Q S, Ma H Z, Wei H C et al. 2014. Holocene lake-level changes of Hurleg Lake on northeastern Qinghai-Tibetan Plateau and possible forcing mechanism. *The Holocene*, **24**(3): 274-283, https://doi.org/10.1177/0959683613517399.

Feng S, Tang M C, Wang D M. 1998. New evidence of the Qinghai-Xizang (Tibet) Plateau as a pilot region of climatic fluctuation in China. *Chinese Science Bulletin*, **43**(6): 633-636, https://doi.org/10.1360/csb1998-43-6-633. (in Chinese)

Folk R L, Ward W C. 1957. Brazos River Bar: a study in the significance of grain size parameters. *Journal of Sedimentary Research*, **27**(1): 3-26, https://doi.org/10.1306/74D70646-2B21-11D7-8648000102C1865D.

Fu X, Zhang J W, Wang L et al. 2016. Recent human impacts on sedimentary record: a case from Lake Toson. *Quaternary Sciences*, **36**(6): 1456-1465, https://doi.org/10.11928/j.issn.1001-7410.2016.06.11. (in Chinese with English abstract)

Hou X Y. 2019. 1:1 million vegetation map of China. National Tibetan Plateau/Third Pole Environment Data Center.

Huang L X, Chen J, Yang K et al. 2023. The northern boundary of the Asian summer monsoon and division of westerlies and monsoon regimes over the Tibetan Plateau in present-day. *Science China Earth Sciences*, **66**(4): 882-893, https://doi.org/10.1007/s11430-022-1086-1.

Huyan Y Y, Yao W S. 2022. Geochemical comparisons of weathering, provenance and tectonics in the fluvial sediments from Yarlung Zangbo to Brahmaputra River. *CATENA*, **210**: 105944, https://doi.org/10.1016/j.catena.2021.105944.

Immerzeel W W, van Beek L P H, Bierkens M F P. 2010. Climate change will affect the Asian water towers. *Science*, **328**(5984): 1382-1385, https://doi.org/10.1126/science.1183188.

Jalil A, Li Y P, Zhang K et al. 2019. Wind-induced hydrodynamic changes impact on sediment resuspension for large, shallow Lake Taihu, China. *International Journal of Sediment Research*, **34**(3): 205-215, https://doi.org/10.1016/j.ijsrc.2018.11.003.

Jiang Y Z, Tang W J, Yang K et al. 2025. Development of a high-resolution near-surface meteorological forcing dataset for the Third Pole region. *Science China Earth Sciences*, **68**(4): 1274-1290, https://doi.org/10.1007/s11430-024-1507-6.

Jiang Y Z, Yang K, Qi Y C et al. 2023. TPHiPr: a long-term (1979-2020) high-accuracy precipitation dataset (1/30°, daily) for the Third Pole region based on high-resolution atmospheric modeling and dense observations. *Earth System Science Data*, **15**(2): 621-638, https://doi.org/10.5194/essd-15-621-2023.

Kasper T, Haberzettl T, Doberschütz S et al. 2012. Indian Ocean Summer Monsoon (IOSM)-dynamics within the past 4 ka recorded in the sediments of Lake Nam Co, central Tibetan Plateau (China). *Quaternary Science Reviews*, **39**: 73-85, https://doi.org/10.1016/j.quascirev.2012.02.011.

Krumbein W C, Pettijohn F J. 1938. Manual of Sedimentary Petrography. D. Appleton-Century Company, New York.

Li D Y, Xu Y H, Wang A J et al. 2015. Analysis of surface

sediment grain size characteristics and modern sedimentary process in Fujian Anhai Gulf. *Acta Sedimentologica Sinica*, **33**(4): 724-734, https://doi.org/10.14027/j.cnki.cjxb.2015.04.011. (in Chinese with English abstract)

Li G Q, Wang X Y, Zhang X J et al. 2022. Westerlies-Monsoon interaction drives out-of-phase precipitation and asynchronous lake level changes between Central and East Asia over the last millennium. *CATENA*, **218**: 106568, https://doi.org/10.1016/j.catena.2022.106568.

Li H Y, Wei H C, Wang C Y et al. 2025. Pollen sedimentary dynamics and hydroclimatic implications in the largest lake system in Qaidam Basin, Northeastern Qinghai-Tibet Plateau. *Palaeogeography*, *Palaeoclimatology*, *Palaeoecology*, **675**: 113115, https://doi.org/10.1016/j.palaeo.2025.113115.

Li W Q, Qian H, Xu P P et al. 2023. Aeolian-fluvial interactions in the Yellow River Basin, China: insights from sedimentary characteristics and provenance of the sedimentary sequences. *Journal of Hydrology*, **624**: 129903, https://doi.org/10.1016/j.jhydrol.2023.129903.

Li X Z, Zhou X, Liu W G et al. 2016. Carbon and oxygen isotopic records from Lake Tuosu over the last 120 years in the Qaidam Basin, Northwestern China: the implications for paleoenvironmental reconstruction. *Global and Planetary Change*, **141**: 54-62, https://doi.org/10.1016/j.gloplacha.2016.04.006.

Ling Y, Dai X Q, Zheng M P et al. 2018. High-resolution geochemical record for the last 1100 yr from Lake Toson, northeastern Tibetan Plateau, and its climatic implications. *Quaternary International*, **487**: 61-70, https://doi.org/10.1016/j.quaint.2017.03.067.

Liu D W, Bertrand S, Villaseñor T et al. 2020. Provenance of northwestern Patagonian river sediments (44-48°S): a critical evaluation of mineralogical, geochemical and isotopic tracers. *Sedimentary Geology*, **408**: 105744, https://doi.org/10.1016/j.sedgeo.2020.105744.

Liu X X, Vandenberghe J, An Z S et al. 2016. Grain size of Lake Qinghai sediments: implications for riverine input and Holocene monsoon variability. *Palaeogeography*, *Palaeoclimatology*, *Palaeoecology*, **449**: 41-51, https://doi.org/10.1016/j.palaeo.2016.02.005.

Liu Y M, Liu X X, Sun Y B. 2021. QGrain: an open-source and easy-to-use software for the comprehensive analysis of grain size distributions. *Sedimentary Geology*, **423**: 105980, https://doi.org/10.1016/j.sedgeo.2021.105980.

Liu Z N, Wang W, Niu Z M et al. 2024. A quantitative method to infer lake area changes based on an extensive survey of lake surface sediment grain size across the Inner Mongolia Plateau, and its application to understanding the evolution of Lake Wulanhushao in northern China since 18.59 cal. kyr BP. *Palaeogeography*, *Palaeoclimatology*, *Palaeoecology*, **641**: 112114, https://doi.org/10.1016/j.palaeo.2024.112114.

Lu H Y, An Z S. 1998. Paleoclimatic significance of grain size of loess-palaeosol deposit in Chinese Loess Plateau. *Science in China Series D*: *Earth Sciences*, **41**(6): 626-631, https://doi.org/10.1007/BF02878745.

Ma S M, Gan F P, Wu H C et al. 2022. ICESat-2 data-based monitoring of 2018-2021 variations in the water levels of lakes in the Qinghai-Tibet Plateau. *Remote Sensing for Natural Resources*, **34**(3): 164-172, https://doi.org/10.6046/zrzyyg.2021329. (in Chinese with English abstract)

Madsen D B, Lai Z P, Sun Y J et al. 2014. Late Quaternary Qaidam lake histories and implications for an MIS 3 "Greatest Lakes" period in northwest China. *Journal of Paleolimnology*, **51**(2): 161-177, https://doi.org/10.1007/s10933-012-9662-x.

Martín-Fernández J A, Barceló -Vidal C, Pawlowsky-Glahn V. 2003. Dealing with zeros and missing values in compositional data sets using nonparametric imputation. *Mathematical Geology*, **35**(3): 253-278, https://doi.org/10.1023/A:1023866030544.

McLennan S M. 1989. Rare earth elements in sedimentary rocks: influence of provenance and sedimentary processes. *Reviews in Mineralogy and Geochemistry*, **21**(1): 169-200.

McManus J. 1988. Grain size determination and interpretation. *In*: Tucker M ed. Techniques in Sedimentology. Blackwell Scientific Publications, Oxford. p.63-85.

Middleton G V. 1976. Hydraulic interpretation of sand size distributions. *The Journal of Geology*, **84**(4): 405-426, https://doi.org/10.1086/628208.

Ming G D, Zhou W J, Wang H et al. 2021. Grain size variation in two lakes from margin of Asian Summer Monsoon and its paleoclimate implications. *Palaeogeography*, *Palaeoclimatology*, *Palaeoecology*, **567**: 110295, https://doi.org/10.1016/j.palaeo.2021.110295.

Mulitza S, Prange M, Stuut J B et al. 2008. Sahel megadroughts triggered by glacial slowdowns of Atlantic meridional overturning. *Paleoceanography*, **23**(4): PA4206, https://doi.org/10.1029/2008PA001637.

Ohta T, Arai H, Noda A. 2011. Identification of the unchanging reference component of compositional data from the properties of the coefficient of variation. *Mathematical Geosciences*, **43**(4): 421-434, https://doi.org/10.1007/s11004-011-9332-y.

Opitz S, Ramisch A, Ijmker J et al. 2016. Spatio-temporal pattern of detrital clay-mineral supply to a lake system on the north-eastern Tibetan Plateau, and its relationship to late Quaternary paleoenvironmental changes. *CATENA*, **137**: 203-218, https://doi.org/10.1016/j.catena.2015.09.003.

Opluštil S, Martínek K, Tasáryová Z. 2005. Facies and architectural analysis of fluvial deposits of the Nýřany Member and the Týnec Formation (Westphalian D-Barruelian) in the Kladno-Rakovník and Pilsen basins. *Bulletin of Geosciences*, **80**(1): 45-66.

OriginLab Corporation. 2020. Origin 2021. Northampton, MA, USA: OriginLab. https://www.originlab.com/.

Pang H L, Gao H S, Eduardo G et al. 2023. Fluvial-aeolian interactions in northern China (Upper Yellow River): implications for provenance and paleoenvironmental interpretations. *CATENA*, **231**: 107257, https://doi.org/10.1016/j.catena.2023.107257.

Paterson G A, Heslop D. 2015. New methods for unmixing sediment grain size data. *Geochemistry*, *Geophysics*, *Geosystems*, **16**(12): 4494-4506, https://doi.org/10.1002/2015GC006070.

Pekel J F, Cottam A, Gorelick N et al. 2016. High-resolution mapping of global surface water and its long-term changes. *Nature*, **540**(7633): 418-422, https://doi.org/10.1038/nature20584.

Peng D D, Zhou T J, Zhang L X et al. 2018. Human contribution to the increasing summer precipitation in Central Asia from 1961 to 2013. *Journal of Climate*, **31**(19): 8005-8021, https://doi.org/10.1175/JCLI-D-17-0843.1.

Poizot E, Méar Y. 2010. Using a GIS to enhance grain size trend analysis. *Environmental Modelling & Software*, **25**(4): 513-525, https://doi.org/10.1016/j.envsoft.2009.10.002.

Pye K. 1987. Aeolian Dust and Dust Deposits. Academic Press, London.

QGIS Development Team. 2016. QGIS Geographic Information System. Open Source Geospatial Foundation. http://qgis.org.

Qiang M R, Chen F H, Zhang J W et al. 2007. Grain size in sediments from Lake Sugan: a possible linkage to dust storm events at the northern margin of the Qinghai-Tibetan Plateau. *Environmental Geology*, **51**(7): 1229-1238, https://doi.org/10.1007/s00254-006-0416-9.

Qin D H, Ding Y H, Su J L et al. 2005. Assessment of climate and environment changes in China (I): climate and environment changes in China and their projection. *Advances in Climate Change Research*, **1**(1): 4-9, https://doi.org/10.3969/j.issn.1673-1719.2005.01.002. (in Chinese with English abstract)

Qiu J. 2008. China: the third pole. *Nature*, **454**(7203): 393-396, https://doi.org/10.1038/454393a.

R Core Team. 2023. R: A Language and Environment for Statistical Computing. R Foundation for Statistical Computing, Vienna, Austria. https://www.R-project.org/.

Shao C K, Yang K, Tang W J et al. 2022. Convolutional neural network-based homogenization for constructing a long-term global surface solar radiation dataset. *Renewable and Sustainable Energy Reviews*, **169**: 112952, https://doi.org/10.1016/j.rser.2022.112952.

Song G, Wang H L, Shi L F. 2020. Climate evolution since 9.32 Cal Ka BP in Keluke Lake, northeastern Qaidam Basin, China. *Journal of Arid Environments*, **178**: 104149, https://doi.org/10.1016/j.jaridenv.2020.104149.

Stauch G, Lai Z P, Lehmkuhl F et al. 2018. Environmental changes during the late Pleistocene and the Holocene in the Gonghe Basin, North-Eastern Tibetan Plateau. *Palaeogeography, Palaeoclimatology, Palaeoecology*, **509**: 144-155, https://doi.org/10.1016/j.palaeo.2016.12.032.

Stuut J B W, Temmesfeld F, De Deckker P. 2014. A 550 ka record of aeolian activity near North West Cape, Australia: inferences from grain-size distributions and bulk chemistry of SE Indian Ocean deep-sea sediments. *Quaternary Science Reviews*, **83**: 83-94, https://doi.org/10.1016/j.quascirev.2013.11.003.

Sun D H, Bloemendal J, Rea D K et al. 2002. Grain-size distribution function of polymodal sediments in hydraulic and aeolian environments, and numerical partitioning of the sedimentary components. *Sedimentary Geology*, **152**(3-4): 263-277, https://doi.org/10.1016/S0037-0738(02)00082-9.

Tang C Y, Li Y P, He C et al. 2020. Dynamic behavior of sediment resuspension and nutrients release in the shallow and wind-exposed Meiliang Bay of Lake Taihu. *Science of the Total Environment*, **708**: 135131, https://doi.org/10.1016/j.scitotenv.2019.135131.

Taylor S R, McLennan S M. 1985. The Continental Crust: Its Composition and Evolution. Blackwell Scientific Publications, Oxford.

The MathWorks Inc. 2019. MATLAB version 9.7.0 (R2019b). Natick, Massachusetts: The MathWorks Inc. https://www.mathworks.com/support/requirements/previous-releases.html.

Tsoar H, Pye K. 1987. Dust transport and the question of desert loess formation. *Sedimentology*, **34**(1): 139-153, https://doi.org/10.1111/j.1365-3091.1987.tb00566.x.

Udden J A. 1914. Mechanical composition of clastic sediments. *Geological Society of America Bulletin*, **25**(1): 655-744, https://doi.org/10.1130/GSAB-25-655.

Vasskog K, Kvisvik B C, Paasche Ø. 2016. Effects of hydrogen peroxide treatment on measurements of lake sediment grain-size distribution. *Journal of Paleolimnology*, **56**(4): 365-381, https://doi.org/10.1007/s10933-016-9924-0.

Walker R G, James N P. 1992. Facies Models: Response to Sea Level Change. Geological Association of Canada, St. John's.

Walling D E, Moorehead P W. 1989. The particle size characteristics of fluvial suspended sediment: an overview. *Hydrobiologia*, **176**(1): 125-149, https://doi.org/10.1007/BF00026549.

Wan W, Xiao P F, Feng X Z et al. 2014. Monitoring lake changes of Qinghai-Tibetan Plateau over the past 30 years using satellite remote sensing data. *Chinese Science Bulletin*, **59**(10): 1021-1035, https://doi.org/10.1007/s11434-014-0128-6.

Wang C, Wang H L, Song G et al. 2019. Grain size of surface sediments in Selin Co (Central Tibet) linked to water depth and offshore distance. *Journal of Paleolimnology*, **61**(2): 217-229, https://doi.org/10.1007/s10933-018-0054-8.

Wang J Z, Wu J L, Zhan S E et al. 2021. Records of hydrological change and environmental disasters in sediments from deep Lake Issyk-Kul. *Hydrological Processes*, **35**(4): e14136, https://doi.org/10.1002/hyp.14136.

Weibull W. 1951. A statistical distribution function of wide applicability. *Journal of Applied Mechanics*, **18**(3): 293-297, https://doi.org/10.1115/1.4010337.

Wentworth C K. 1922. A scale of grade and class terms for clastic sediments. *The Journal of Geology*, **30**(5): 377-392, https://doi.org/10.1086/622910.

Wünnemann B, Yan D D, Hu S et al. 2023. Seasonal variations in surface processes and hydroclimate on an alpine lake, NE Tibetan Plateau. *Quaternary Science Reviews*, **300**: 107876, https://doi.org/10.1016/j.quascirev.2022.107876.

Xiao J L, Chang Z G, Fan J W et al. 2012. The link between grain-size components and depositional processes in a

modern clastic lake. *Sedimentology*, **59**(3): 1050-1062, https://doi.org/10.1111/j.1365-3091.2011.01294.x.

Xiao J L, Fan J W, Zhai D Y et al. 2015. Testing the model for linking grain-size component to lake level status of modern clastic lakes. *Quaternary International*, **355**: 34-43, https://doi.org/10.1016/j.quaint.2014.04.023.

Xiao S, Chen F H, Qiang M R et al. 2007. Distribution pattern of grain size in surface sediments from Sugan Lake and its potential in recording aeolian dust in arid China. *Acta Geographica Sinica*, **62**(11): 1153-1164, https://doi.org/10.3321/j.issn:0375-5444.2007.11.004. (in Chinese with English abstract)

Xu F L, Zhang G Q, Woolway R I et al. 2024. Widespread societal and ecological impacts from projected Tibetan Plateau lake expansion. *Nature Geoscience*, **17**(6): 516-523, https://doi.org/10.1038/s41561-024-01446-w.

Xu X D, Dong L L, Zhao Y et al. 2019. Effect of the Asian water tower over the Qinghai-Tibet Plateau and the characteristics of atmospheric water circulation. *Chinese Science Bulletin*, **64**(27): 2830-2841, https://doi.org/10.1360/TB-2019-0203. (in Chinese with English abstract)

Yamaguchi N, Ando T, Enokida H et al. 2024. Logratio analysis of components separated from grain-size distributions and implications for sedimentary processes: an example of bottom surface sediments in a shallow lake. *Sedimentology*, **71**(4): 1291-1304, https://doi.org/10.1111/sed.13174.

Yang K, Jiang Y, Tang W et al. 2023. A high-resolution near-surface meteorological forcing dataset for the Third Pole Region (TPMFD, 1979-2023). National Tibetan Plateau/Third Pole Environment Data Center, https://doi.org/10.11888/Atmos.tpdc.300398.

Yao T D, Bolch T, Chen D L et al. 2022. The imbalance of the Asian water tower. *Nature Reviews Earth & Environment*, **3**(10): 618-632, https://doi.org/10.1038/s43017-022-00299-4.

Yao T D, Thompson L G, Mosbrugger V et al. 2012. Third pole environment (TPE). *Environmental Development*, **3**: 52-64, https://doi.org/10.1016/j.envdev.2012.04.002.

Yu L P, Lai Z P. 2012. OSL chronology and palaeoclimatic implications of aeolian sediments in the eastern Qaidam Basin of the northeastern Qinghai-Tibetan Plateau. *Palaeogeography, Palaeoclimatology, Palaeoecology*, **337-338**: 120-129, https://doi.org/10.1016/j.palaeo.2012.04.004.

Yu Y F, You Q L, Zhang Y Q et al. 2024. Integrated warm-wet trends over the Tibetan Plateau in recent decades. *Journal of Hydrology*, **639**: 131599, https://doi.org/10.1016/j.jhydrol.2024.131599.

Yu Y H, Jin Y Y, Xu D K et al. 2021. Vegetational and climatic changes in the Hurleg Lake, Qinghai, during the last 14000 years. *Quaternary Sciences*, **41**(5): 1229-1243, https://doi.org/10.11928/j.issn.1001-7410.2021.05.01. (in Chinese with English abstract)

Zhang G Q, Yao T D, Xie H J et al. 2020. Response of Tibetan Plateau lakes to climate change: trends, patterns, and mechanisms. *Earth-Science Reviews*, **208**: 103269, https://doi.org/10.1016/j.earscirev.2020.103269.

Zhang J, Xu H, Lan J H et al. 2022. Prolonged drought enhances northwest China dust storm activity. *Journal of Geophysical Research*: *Atmospheres*, **127**(20): e2022JD037088, https://doi.org/10.1029/2022JD037088.

Zhao C, Yu Z C, Zhao Y et al. 2010a. Holocene millennial-scale climate variations documented by multiple lake-level proxies in sediment cores from Hurleg Lake, northwest China. *Journal of Paleolimnology*, **44**(4): 995-1008, https://doi.org/10.1007/s10933-010-9469-6.

Zhao J J, Li X Z, He Y X et al. 2022. Opposing industrial era moisture patterns between basins and mountains in southern arid Central Asia. *CATENA*, **215**: 106367, https://doi.org/10.1016/j.catena.2022.106367.

Zhao Y, Yu Z C, Chen F H et al. 2007. Holocene vegetation and climate history at Hurleg Lake in the Qaidam Basin, northwest China. *Review of Palaeobotany and Palynology*, **145**(3-4): 275-288, https://doi.org/10.1016/j.revpalbo.2006.12.002.

Zhao Y, Yu Z C, Liu X J et al. 2010b. Late Holocene vegetation and climate oscillations in the Qaidam Basin of the northeastern Tibetan Plateau. *Quaternary Research*, **73**(1): 59-69, https://doi.org/10.1016/j.yqres.2008.11.007.

Zhou J C, Wu J L, Zeng H A. 2018. Extreme flood events over the past 300 years inferred from lake sedimentary grain sizes in the Altay Mountains, northwestern China. *Chinese Geographical Science*, **28**(5): 773-783, https://doi.org/10.1007/s11769-018-0968-0.

Zhou J C, Wu J L, Zhang H L et al. 2022. Late Quaternary hydroclimate change inferred from lake sedimentary record in arid central Asia. *Boreas*, **51**(3): 573-583, https://doi.org/10.1111/bor.12573.

Zhou S, Zhang J W, Cheng B et al. 2024. Holocene pollen record from Lake Gahai, NE Tibetan Plateau and its implications for quantitative reconstruction of regional precipitation. *Quaternary Science Reviews*, **326**: 108504, https://doi.org/10.1016/j.quascirev.2024.108504.

Electronic supplementary material

Supplementary material (Supplementary Tables S1–S2 and Figs.S1–S3) is available in the online version of this article at https://doi.org/10.1007/s00343-025-5260-4.